PAPER

Check for updates

Synthesis, structure, and superconductivity of La$_{7+2x}$Sr$_{1-4x}$K$_x$Na$_x$Cu$_4$O$_{16-\delta}$†

Deyang Xu,[a] Guohong Cai,[b] Peiliang Huang,[c] Xi Wu,[d] Yan Wang,[b] Jinling Geng,[b] Jing Ju, [ID][b] Xiaoge Wang,[b] Congling Yin [ID] *[a] and Guobao Li [ID] *[b]

Sodium and potassium have been doped into La$_7$SrCu$_4$O$_{16-\delta}$ to form La$_{7+2x}$Sr$_{1-4x}$K$_x$Na$_x$Cu$_4$O$_{16-\delta}$ solid solutions by a solid-state reaction, which crystallizes in the *I4/mmm* space group when $0 \leq x < 0.16$ and *Fmmm* when $0.16 < x \leq 0.25$. With the equivalent replacement of four Sr^{2+} by one Na$^+$, one K$^+$ and two La^{3+}, it is very interesting to find that T_c^{zero} (the definition is presented in the introduction part) of La$_{7+2x}$Sr$_{1-4x}$K$_x$Na$_x$Cu$_4$O$_{16-\delta}$ does not remain constant with an increase in x but first increases from 14.8 K for $x = 0.00$ to 33.9 K for $x = 0.10$ and then decreases to 18.5 K for $x = 0.175$.

1. Introduction

Since J. G. Bednorz *et al.*[1] first discovered superconductivity in the La–Ba–Cu–O system with T_c^{onset} (a transition temperature at which the resistivity begins to drop rapidly to "zero" with a decrease in temperature, indicating the onset of superconductivity) at about 30 K and T_c^{zero} (the highest temperature at which the resistivity of the sample reaches "zero", marking the full superconducting state) at about 20 K, the mechanism of high T_c (a general term for the phase transition temperature, which can be one of T_c^{onset}, T_c^{zero}, and T_c^{mag} (the temperature at which the magnetization of the sample starts to decrease to negative values with a decrease of temperature, indicating the start of the Meissner effect) for a superconductor) has been widely investigated, and new materials with higher T_c have been explored.[2,3] La$_2$CuO$_{4-\delta}$ materials are called "model materials" for the study of superconductivity due to their simple formulation and structure,[4] which provides a unique opportunity to investigate the relationship between the structure and superconducting properties.[5] The widely studied Sr-substituted compound La$_{2-x}$Sr$_x$CuO$_{4-\delta}$ is the copper oxide compound that can be varied over a wide enough range to obtain a full spectrum of electronic properties.[6] As the Sr content increases,

it goes from antiferromagnetic insulator ($0 \leq x \leq 0.03$) to superconductor ($0.07 \leq x \leq 0.27$) to non-superconducting metal ($x \geq 0.27$).[7] Many attempts have been made to investigate the relationship with T_c in La$_{2-x}$Sr$_x$CuO$_{4-\delta}$ systems by adding new doping elements and changing the doping amount. J. P. Attfield *et al.*[8] have shown that the T_c of (Ln$_{1-x}$M$_x$)$_2$CuO$_{4-\delta}$ (Ln = La and other lanthanides, M = Ca, Sr, and Ba) superconductors depends on the doping level x and the average A-site cation radius.[9,10] More complex doping compounds, such as (La$_{0.925}$Sr$_{0.075-x}$Ba$_x$)$_2$CuO$_{4-\delta}$,[11] (La$_{0.925-x}$Ln$_x$Sr$_{0.075}$)$_2$CuO$_{4-\delta}$ (Ln = Pr, Nd, Sm, Eu),[10,12] have also been studied, which indicates that T_c is also affected by the change in the ionic radius at the A-site. M. A. Subramanian *et al.*[13] have reported the superconductivity of La$_{2-x}$A$_x^{1+}$CuO$_{4-\delta}$ (A = Na, K) with T_c^{onset} ~40 K, which confirms the feasibility of A-site doping with alkali metal cations. The elements Na and K can influence the crystal structure and electronic properties of copper oxide superconductors due to their unique electronic configurations.[14,15] They also help to lower the sintering temperature, promote sintering, and inhibit grain growth.[16] Therefore, combining Na and K into La$_{2-x}$Sr$_x$CuO$_{4-\delta}$ matrices provides an interesting avenue to tailor the electronic structure and superconducting properties of the materials. In the La$_{2-x}$Sr$_x$CuO$_{4-\delta}$ system, superconductivity is usually reported when $0.05 < x < 0.27$, $x = 0.15$, which is identified as the optimal doping concentration.[17] Many studies relating to the optimal doping of La$_{1.85}$Sr$_{0.15}$CuO$_{4-\delta}$ have been performed.[18–22] The research on the over-doped range ($0.15 \leq x \leq 0.27$) should be enhanced. Therefore, La$_{1.75}$Sr$_{0.25}$CuO$_{4-\delta/4}$ (which can also be noted as La$_7$SrCu$_4$O$_{16-\delta}$) is chosen as the solid solution matrix, serving as a starting point for further investigation. To reduce the change in the average A-site cation radius to limit the size effect on T_c suggested by J. P. Attfield *et al.*,[8] one K$^+$, one Na$^+$, and two La^{3+} were chosen to replace four Sr^{2+} (the details are shown in section 3.1). Then, the nominal compounds La$_{7+2x}$Sr$_{1-4x}$K$_x$Na$_x$Cu$_4$O$_{16-\delta}$ were tried. In this case,

[a]MOE Key Laboratory of New Processing Technology for Nonferrous Metal and Materials, Guangxi Key Laboratory of Optical and Electronic Materials and Devices, College of Materials Science and Engineering, Guilin University of Technology, Guilin 541004, People's Republic of China

[b]Beijing National Laboratory for Molecular Sciences, State Key Laboratory of Rare Earth Materials Chemistry and Applications, College of Chemistry and Molecular Engineering, Peking University, Beijing, 100871, People's Republic of China

[c]Beijing Ritan High School, Beijing, 100020, People's Republic of China

[d]Henan Institute of Chemical Technology, Kaifeng, 475000, People's Republic of China. E-mail: congling.yin@glut.edu.cn; liguobao@pku.edu.cn

† Electronic supplementary information (ESI) available. See DOI: https://doi.org/10.1039/d4ra06045h

it is found that the above doping is just an equivalent doping, which introduces no additional electron or hole into the synthesized compound if δ is not changed. This means that the T_c of $La_{7+2x}Sr_{1-4x}K_xNa_xCu_4O_{16-\delta}$ may remain constant if we believe that the T_c of doped $La_2CuO_{4-\delta}$ is strongly related to the hole content. However, the T_c^{zero} of $La_{7+2x}Sr_{1-4x}K_xNa_xCu_4O_{16-\delta}$ is raised to 33.9 K for $x = 0.10$ from 14.8 K for $x = 0.00$, then finally lowered to 18.5 K for $x = 0.175$. The details for such an interesting phenomenon and the possible explanation about the influence of K and Na ions on the superconductivity are presented below.

2. Experimental

The samples with the nominal formula $La_{7+2x}Sr_{1-4x}K_xNa_xCu_4O_{16-\delta}$ ($x = 0.0$, 0.025, 0.050, 0.075, 0.100, 0.125, 0.150, 0.175, 0.200, 0.225 and 0.250, denoted as LSKNCO1, LSKNCO2, …, and LSKNCO11, respectively) were synthesized. La_2O_3 (99.95%), $SrCO_3$ (A.R.), K_2CO_3 (A.R.), Na_2CO_3 (A.R.), and CuO (A.R.) were used as raw materials. The oven-dried raw materials were weighed according to the molar ratios of the nominal formula $La_{7+2x}Sr_{1-4x}K_xNa_xCu_4O_{16-\delta}$ and homogenized by about 30 min of grinding for total 10 g of mixtures with an agate mortar and a pestle. These mixtures were sintered first at 900 °C for 12 h. Then, the reacted powders were pressed into pellets under 30 MPa and sintered at 920 °C for 12 h. The sintered mass was again crushed, pulverized, and pressed into cylindrical pellets to undertake five 12 h heat treatments at 1100 °C (LSKNCO1, LSKNCO2, LSKNCO3), 1080 °C (LSKNCO4, LSKNCO5), 1060 °C (LSKNCO6), 1020 °C (LSKNCO7), and 960 °C (LSKNCO8, LSKNCO9, LSKNCO10, LSKNCO11). All the treatments were performed in air.

Powder X-ray diffraction (PXRD) data of $La_{7+2x}Sr_{1-4x}K_xNa_xCu_4O_{16-\delta}$ were collected on a PANalytical X'Pert PRO (The Netherlands) with Cu Kα ($\lambda1 = 1.5405$ Å and $\lambda2 = 1.5443$ Å) radiation over a wide 2θ range (5°–120°) at a scan rate of 1° per minute. Time-of-flight (TOF) neutron powder diffraction (NPD) data were collected for the samples LSKNCO2, LSKNCO5, and LSKNCO9 using the General-Purpose Powder Diffractometer (GPPD) at the China Scattering Neutron Source (CSNS, Dongguan, China). Rietveld refinements were performed for the XRD patterns and neutron diffraction patterns using TOPAS-Academic software.[23] Selected area electron diffraction (SAED) was performed on a JEM2100 (accelerating voltage: 200 kV). X-ray photoelectron spectroscopy (XPS) was carried out using a Kratos Axis Ultra spectrometer (UK) at a voltage of 15 kV and a current of 15 mA. The vacuum of the instrument during the test was about 10^{-10} mbar, and the chamber pressure was not greater than 5.0×10^{-9} torr. All the acquired energy spectral data were calibrated with the C 1s emission at $E_b = 284.8$ eV. Direct-current (dc) magnetic susceptibility was recorded in a magnetic field of 10 Oe while heating the sample from 2 K to 300 K after zero-field cooling (ZFC) and field cooling (FC) using an MPMS-3 Superconducting Quantum Interference Device (SQUID, Quantum Design) magnetometer. The resistivity was investigated with a cryogenic liquid helium-free physical property measurement system

(PPMS, supplied by East Changing, China) from 2 to 120 K. Scanning electron microscopy (SEM) imaging and elemental analysis through energy-dispersive X-ray spectroscopy (EDS) were performed using an SU8600 (Hitachi, Japan) field-emission scanning electron microscope equipped with an XFlash 760 (Bruker, Germany) EDS spectrometer.

3. Results and discussion

3.1 Solid solution and structure of $La_{7+2x}Sr_{1-4x}K_xNa_xCu_4O_{16-\delta}$

The powder XRD patterns of samples LSKNCO1 to LSKNCO11 are depicted in Fig. 1. The powder XRD patterns of LSKNCO2 to LSKNCO7 closely resemble that of LSKNCO1 ($La_{1.75}Sr_{0.25}CuO_{4-\delta/4}$), suggesting a similarity in their structures to $La_{1.75}Sr_{0.25}CuO_{4-\delta/4}$, which was reported to crystallize in a tetragonal space group.[17] When more Na and K are doped into the compound, some reflection peaks are split, as shown at the right hand of Fig. 1, at 2 theta of about 33.5° for the samples LSKNCO8 to LSKNCO11, which may mean that these samples crystalize in the orthogonal space group, similar as that of $La_2CuO_{4-\delta}$.[3] Therefore, the structures of $La_{1.75}Sr_{0.25}CuO_{4-\delta/4}$ and $La_2CuO_{4-\delta}$ were used as the starting structure in the Rietveld refinement of the X-ray diffraction patterns of LSKNCO1 to LSKNCO7 and LSKNCO8 to LSKNCO11, respectively. Reasonable refinement results were obtained with $R_p^x \leq 0.032$, $R_{wp}^x \leq 0.045$. Neutron diffraction data of the selected samples LSKNCO2 (tetragonal phase), LSKNCO5 (tetragonal phase), and LSKNCO9 (orthogonal phase) were obtained and are refined well using the same lattice parameters and atomic coordination as those used in the refinement of the X-ray diffraction patterns for the corresponding samples with $R_p^n \leq 0.048$, $R_{wp}^n \leq 0.062$, which confirms that the results obtained from the X-ray diffraction data are plausible. Typical Rietveld plots of the X-
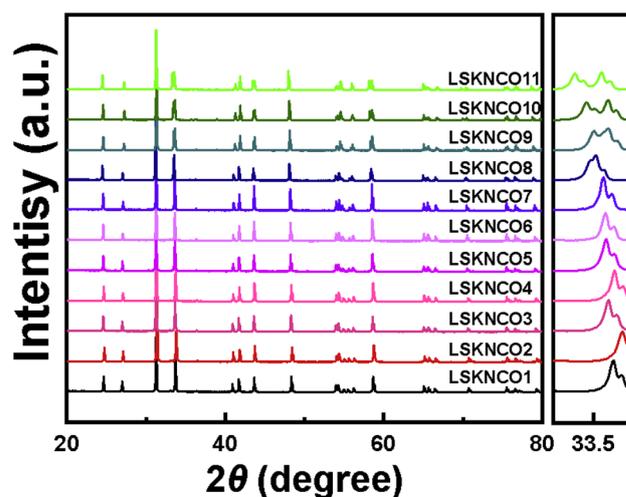

Fig. 1 X-ray diffraction data of $La_{7+2x}Sr_{1-4x}K_xNa_xCu_4O_{16-\delta}$. ($x = 0.000$ (LSKNCO1), 0.025 (LSKNCO2), 0.050 (LSKNCO3), 0.075 (LSKNCO4), 0.100 (LSKNCO5), 0.125 (LSKNCO6), 0.150 (LSKNCO7), 0.175 (LSKNCO8), 0.200 (LSKNCO9), 0.225 (LSKNCO10) and 0.250 (LSKNCO11)).

ray and neutron diffraction data for $La_{7+2x}Sr_{1-4x}K_xNa_xCu_4O_{16-\delta}$ with $x = 0.1$ and 0.2 are shown in Fig. 2 and the corresponding refinement details are listed in Table 1 (the others are shown in Fig. S1 to S9 and Tables S1 to S4 in ESI†).

Through the Rietveld refinement, the lattice parameters and unit cell volume of $La_{7+2x}Sr_{1-4x}K_xNa_xCu_4O_{16-\delta}$ were obtained and are presented in Fig. 3, where the data corresponding to the $\sqrt{2}a_T$ and $2V_T$ of the tetragonal phase were used to simplify the comparison. The lattice parameter a of the tetragonal $La_{7+2x}Sr_{1-4x}K_xNa_xCu_4O_{16-\delta}$ phase (noted as a_T) increases with an increase in the Na and K content until $x \approx 0.16$. When $x > 0.16$, the orthogonal $La_{7+2x}Sr_{1-4x}K_xNa_xCu_4O_{16-\delta}$ phase appears. The lattice parameters a and b of the $La_{7+2x}Sr_{1-4x}K_xNa_xCu_4O_{16-\delta}$ phase (noted as a_o and b_o, respectively) also increase with an increase in the Na and K content. The lattice parameter c of the tetragonal $La_{7+2x}Sr_{1-4x}K_xNa_xCu_4O_{16-\delta}$ (c_T) and the orthogonal $La_{7+2x}Sr_{1-4x}K_xNa_xCu_4O_{16-\delta}$ (c_o) are similar to each other, as shown in Fig. 3b. They decrease in a different slope with the increase in the Na and K content in the samples with $x = 0.16$ as the boundary. Simultaneously, the unit cell volume of the tetragonal $La_{7+2x}Sr_{1-4x}K_xNa_xCu_4O_{16-\delta}$ and the orthogonal $La_{7+2x}Sr_{1-4x}K_xNa_xCu_4O_{16-\delta}$ increases in a different slope before

and after $x = 0.16$. Therefore, the tetragonal to orthogonal phase transition occurs at about $x = 0.16$ for the $La_{7+2x}Sr_{1-4x}K_xNa_xCu_4O_{16-\delta}$ system.

It is known that La, Sr, Na, K in $La_{7+2x}Sr_{1-4x}K_xNa_xCu_4O_{16-\delta}$ are situated at the same crystallographic site (noted as the La site here), which is nine-coordinated to oxygen atoms in the $I4/mmm$ or $Fmmm$ space group. Therefore, the radius of La^{3+}, Sr^{2+}, Na^+, and K^+ under nine-coordination is used to consider the change in the lattice parameters, which are 1.212 Å, 1.31 Å, 1.24 Å, and 1.55 Å, respectively. The change Δ in the average radius of La site is denoted as follows.

$$\Delta = (2r_{La^{3+}} (IX) + r_{K^+} (IX) + r_{Na^+} (IX) - 4r_{Sr^{2+}} (IX)) \, x/4$$
$$= -0.0065x \, (\text{Å}) \tag{1}$$

Eqn (1) indicates that the average radius of the La site should decrease with an increase in the Na and K contents in the samples, which will reduce the volume of the unit cell of the sample. However, the data shown in Fig. 3b tell us that the volume of the unit cell of $La_{7+2x}Sr_{1-4x}K_xNa_xCu_4O_{16-\delta}$ increases with an increase in the Na and K contents in the sample, which means that the radius data for La^{3+}, Sr^{2+}, Na^+, and K^+ under
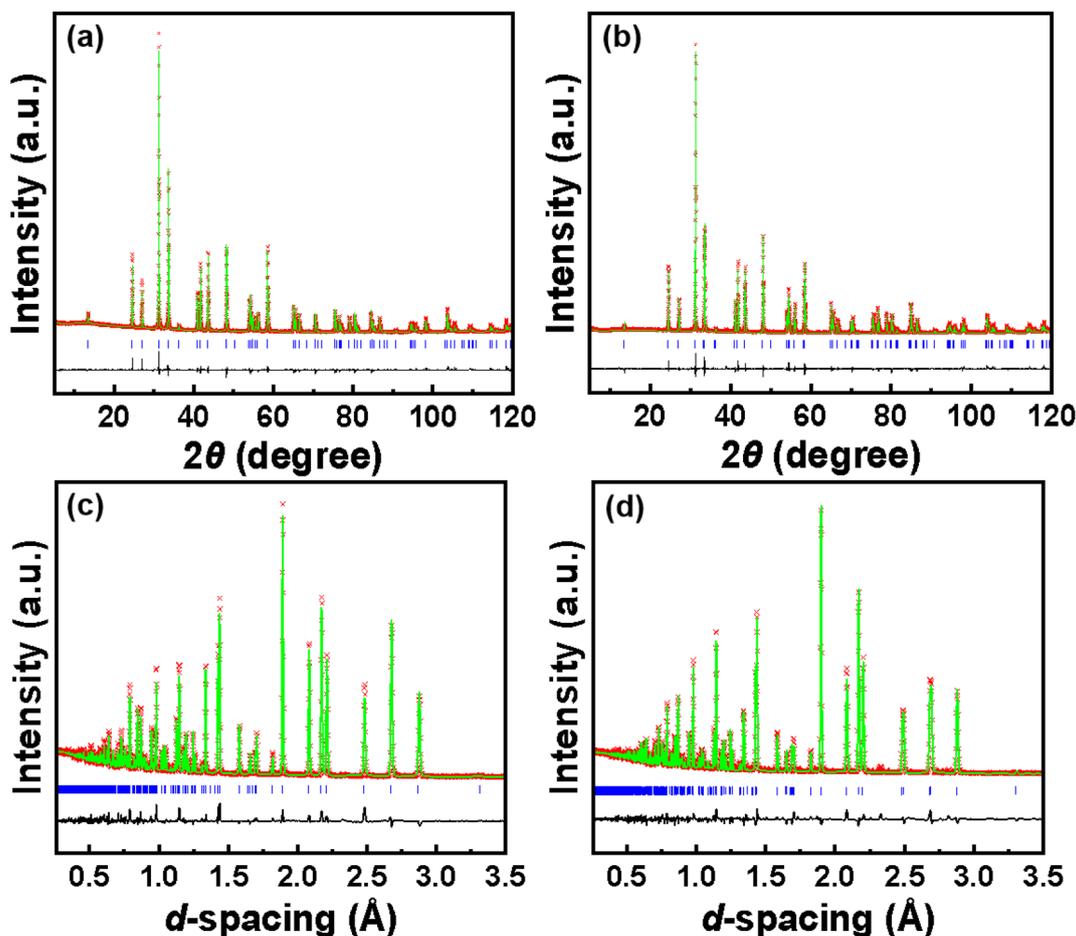

Fig. 2 Rietveld plot of the X-ray (a) LSKNCO5; (b) LSKNCO9 and neutron diffraction data (c) LSKNCO5; (d) LSKNCO9. The plus symbol represents the observed value, the solid line presents the calculated value, the marks below the diffraction patterns are the calculated reflection positions, and the difference curve is shown at the bottom in the figure.

Table 1 Rietveld refinement details of $La_{7+2x}Sr_{1-4x}K_xNa_xCu_4O_{16-\delta}$ with $x = 0.100$ and 0.200

Sample	LSKNCO5, $x = 0.100$	LSKNCO9, $x = 0.200$
Lattice parameters (Å)	$a = b = 3.7781(2)$, $c = 13.2411(5)$	$a = 5.3540(2)$, $b = 5.3769(1)$, $c = 13.1962(5)$
Space group	$I4/mmm$	$Fmmm$
Atom	(x, y, z)	(x, y, z)
La/Sr/K/Na[a]	0, 0, 0.3609(3)	0, 0, 0.3611(3)
Cu1	0, 0, 0	0, 0, 0
O1	0, 1/2, 0	1/4, 1/4, 0
O2	0, 0, 0.1814(6)	0, 0, 0.1867(8)
B_{eq}(La/Sr/K/Na) (Å²)[b]	1.02(1)	0.65(1)
B_{eq}(Cu) (Å²)	1.29(1)	0.99(1)
B_{eq}(O1) (Å²)	1.17(1)	0.55(1)
B_{eq}(O2) (Å²)	2.13(1)	2.42(2)
R factor[c]	$R_{wp}^x = 0.040$, $R_{wp}^n = 0.062$, $R_p^x = 0.020$, $R_p^n = 0.044$	$R_{wp}^x = 0.044$, $R_{wp}^n = 0.054$, $R_p^x = 0.032$, $R_p^n = 0.048$

[a] The occupancy of La/Sr/K/Na is $0.9000 : 0.0750 : 0.0125 : 0.0125$ for $x = 0.100$, and $0.925 : 0.025 : 0.025 : 0.025$ for $x = 0.200$. [b] B_{eq} is the thermal displacement parameter. [c] R_{wp}^x and R_{wp}^n are the weighted R factors calculated by $(\text{sum}(w(I_0 - I_c)^2)/\text{sum}(w(I_0^2)))^{0.5}$ for powder X-ray and neutron diffraction data, respectively; R_p^x and R_p^n are the R factors calculated by $\text{sum}(|I_0 - I_c|/\text{sum}(I_0)$ for powder X-ray and neutron diffraction data, respectively.

nine-coordination are not suitable for the present compound $La_{7+2x}Sr_{1-4x}K_xNa_xCu_4O_{16-\delta}$. For the $La_{7+2x}Sr_{1-4x}K_xNa_xCu_4O_{16-\delta}$ system, the average radius of the La site should increase with four Sr^{2+} replaced by two La^{3+}, one Na^+ and one K^+. Then, the increase in the lattice parameters a_T, a_o, and b_o can be attributed to this increase in the average radius of the La site. The decrease in the lattice parameters c_T and c_o may be explained by the "shrinkage effect": expansion of the a_T, a_o, and b_o axis allows the layers to be closer together to shrink the c_T and c_o axis. This phenomenon is similar to the findings in $ZrSi_{1-x}Ge_xTe$ solid solutions by C. Wang et al.[24] A. Kimura et al. also found that on adding larger Cr and Ti atoms into the AlN lattice, the hexagonal lattice spacings expanded in the a-direction and shrank in the c-direction.[25]

It was found that the lattice parameter a of $La_{2-x}Sr_xCuO_{4-\delta}$ $(0.1 \leq x \leq 0.25)$ reported by J. M. Tarascon[26] also decreases with an increase in Sr, which is very similar to that of our $La_{7+2x}Sr_{1-4x}K_xNa_xCu_4O_{16-\delta}$ samples (shown in Fig. S10†). However, the lattice parameter c and the unit cell volume of $La_{2-x}Sr_xCuO_{4-\delta}$ are smaller than those of $La_{7+2x}Sr_{1-4x}K_xNa_xCu_4O_{16-\delta}$ with the same amount of Sr in the

sample (shown in Fig. S10†), which supports that K^+ and Na^+ should occupy the La sites as these larger ions expand the lattice (see ESI† for the details).

The SAED (selected-area electron diffraction) patterns are very useful to check the choice of the space group for the studied materials.[27,28] Therefore, the SAED patterns of the selected samples in the $La_{7+2x}Sr_{1-4x}K_xNa_xCu_4O_{16-\delta}$ system have been obtained with the typical data shown in Fig. 4 for LSKNCO5. The tetragonal space group $I4/mmm$ with lattice parameters $a \approx 3.778$ Å, $b \approx 3.778$ Å, $c \approx 13.241$ Å, $\alpha = 90°$, $\beta = 90°$, $\gamma = 90°$ can adequately index the corresponding points, indicating that the space group $I4/mmm$ can be used to describe the structures of LSKNCO5. As the X-ray diffraction patterns of LSKNCO1 to LSKNCO7 are almost the same as that of LSKNCO5, the space group $I4/mmm$ can also be used to describe the structures of LSKNCO1 to LSKNCO7.

In order to access the contents of Na and K in $La_{7+2x}Sr_{1-4x}K_xNa_xCu_4O_{16-\delta}$, EDX analysis was performed on LSKNCO9 and LSKNCO11 (see Fig. S11 and S12†). It was found that the La : Sr : K : Na : Cu ratio of LSKNCO9 was $27.88 : 0.68 : 0.76 : 0.82 : 15.76$ (corresponding to $7.34 : 0.18 : 0.20 : 0.22 :$
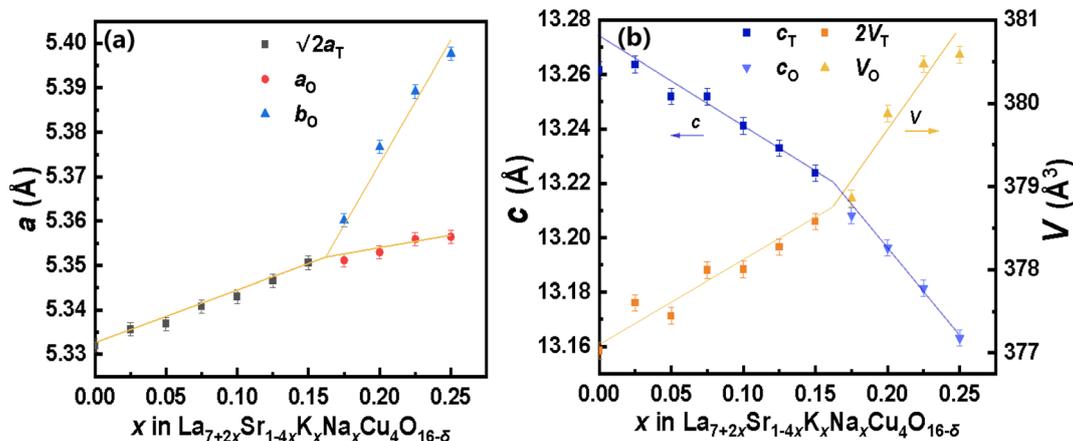

Fig. 3 Lattice parameters of $La_{7+2x}Sr_{1-4x}K_xNa_xCu_4O_{16-\delta}$ $(0 \leq x \leq 0.25)$. a_T, c_T, V_T, the lattice parameter a, c, and the volume of unit cell for the tetragonal phase; a_o, b_o, c_o, V_o, the lattice parameter a, b, c, and the volume of the unit cell for the orthogonal phase.
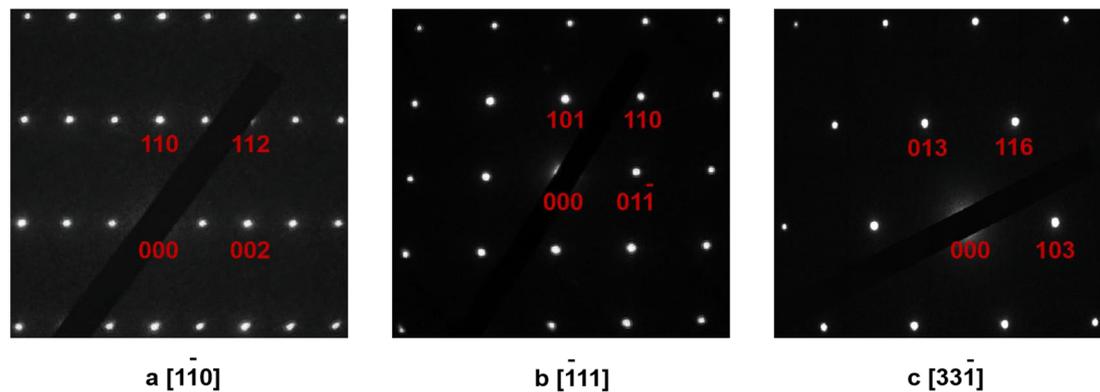

Fig. 4 The electron diffraction patterns of LSKNCO5 ($La_{7+2x}Sr_{1-4x}K_xNa_xCu_4O_{16-\delta}$ with $x = 0.1$) along [331] (a), [111] (b) and [110] (c) indexed by space group $I4/mmm$ with $a \approx 3.778$ Å, $b \approx 3.778$ Å, $c \approx 13.241$ Å, $\alpha = 90°$, $\beta = 90°$ and $\gamma = 90°$.

4.15), and the La : K : Na : Cu ratio of LSKNCO11 was 28.23 : 0.82 : 0.94 : 14.70 (corresponding to 8.02 : 0.23 : 0.27 : 4.18), which are essentially identical to their ideal values. Therefore, the chemical composition of the samples aligns with the planned formula.

3.2 Valence of Na and Cu in $La_{7+2x}Sr_{1-4x}K_xNa_xCu_4O_{16-\delta}$

As widely recognized, copper in most copper oxides exists in the oxidation states of +1, or +2. However, the presence of Sr^{2+}, Na^+, and K^+ in $La_{7+2x}Sr_{1-4x}K_xNa_xCu_4O_{16-\delta}$ can induce the partial oxidation of Cu^{2+} to Cu^{3+}. In order to accurately understand the changes in the oxidation state of copper in the samples, the X-ray photoelectron spectroscopy (XPS) data of the samples LSKNCO1, LSKNCO3, LSKNCO5, LSKNCO7, LSKNCO9, and LSKNCO11 was obtained. The full-scan XPS measurement spectrum of the LSKNCO9 sample is presented in Fig. 5a, which

indicates the presence of La, Sr, K, Na, Cu, and O elements in the sample (with C being introduced by the XPS instrument itself). High-resolution element-specific fine scans of Na 1s, Cu 2p, and O 1s were recorded, which will be discussed in detail later.

As shown in Fig. 5b, Na 1s XPS have no significant signals for the samples LSKNCO1 and LSKNCO3. This is probably due to the low doping concentration of Na^+. As the Na content in the samples increases, prominent peaks are observed at an energy position of about 1071.58 eV in LSKNCO5, LSKNCO7, LSKNCO9, and LSKNCO11, corresponding to the Na 1s orbital. The Na^+ state (binding energy ~1071.0–1071.5 eV) can be confirmed based on the commonly used line position diagrams.[29,30] Due to the limited sensitivity of the spectrometer to K elements, the signal intensity for K is not significant, and the spectra for K elements were not measured.

Fig. 5c shows the Cu 2p XPS spectra of all the studied components containing Cu $2p_{3/2}$ and Cu $2p_{1/2}$ as well as satellite peaks. The main peaks with binding energies at ~933.14 eV and ~952.62 eV correspond to Cu^{2+} at Cu $2p_{3/2}$ and Cu $2p_{1/2}$, respectively.[31–33] However, the peaks at higher energies of the binding energy at ~934.98 eV and ~954.63 eV correspond to the Cu^{3+} of Cu $2p_{3/2}$ and Cu $2p_{1/2}$, respectively.[31] Rocking satellite peaks at binding energies 940.79 eV and 943.31 eV were observed, which can be assigned to Cu^{2+} and Cu^{3+}, respectively. The $Cu^{2+} : Cu^{3+}$ ratios in these samples were obtained by fitting the XPS spectra of Cu 2p, as shown in Fig. 5d, which are listed in Table 2 and presented in Fig. 6. The $Cu^{2+} : Cu^{3+}$ ratio of the
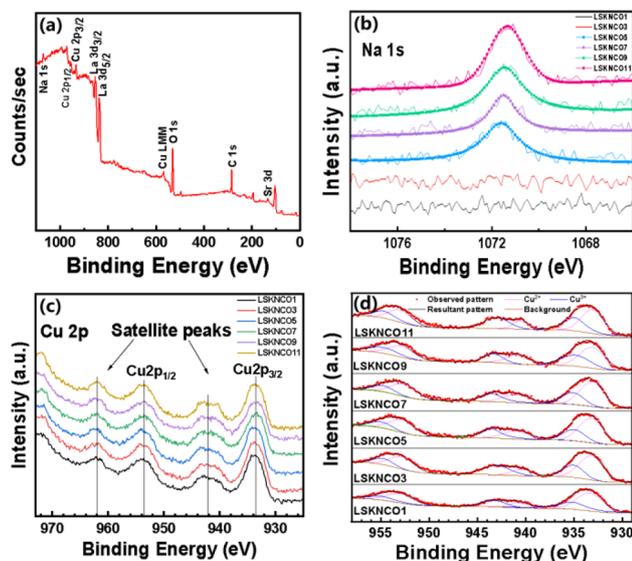

Fig. 5 Full scan spectra of LSKNCO9 (a), and the XPS spectra of Na 1s (b), Cu $2p_{3/2}$ and Cu $2p_{1/2}$ (c), the Cu $2p_{3/2}$ and Cu $2p_{1/2}$ XPS peak fitted with three different Gaussian peaks (d) for LSKNCO1, LSKNCO3, LSKNCO5, LSKNCO7, LSKNCO9 and LSKNCO11.

Table 2 Binding energies (eV) of Cu $2p_{3/2}$, Cu $2p_{1/2}$, and the $Cu^{2+} : Cu^{3+}$ ratio for $La_{7+2x}Sr_{1-4x}K_xNa_xCu_4O_{16-\delta}$

	$2p_{3/2}$		$2p_{1/2}$		$Cu^{2+} : Cu^{3+}$
Sample	Cu^{2+}	Cu^{3+}	Cu^{2+}	Cu^{3+}	
LSKNCO1	933.40	935.19	953.00	954.90	0.47 : 0.53
LSKNCO3	933.20	935.04	952.79	954.76	0.70 : 0.30
LSKNCO5	933.22	935.00	952.81	954.96	0.83 : 0.17
LSKNCO7	933.14	935.10	952.62	954.76	0.72 : 0.28
LSKNCO9	933.11	934.86	952.85	954.76	0.62 : 0.38
LSKNCO11	933.10	934.98	952.98	954.63	0.54 : 0.46
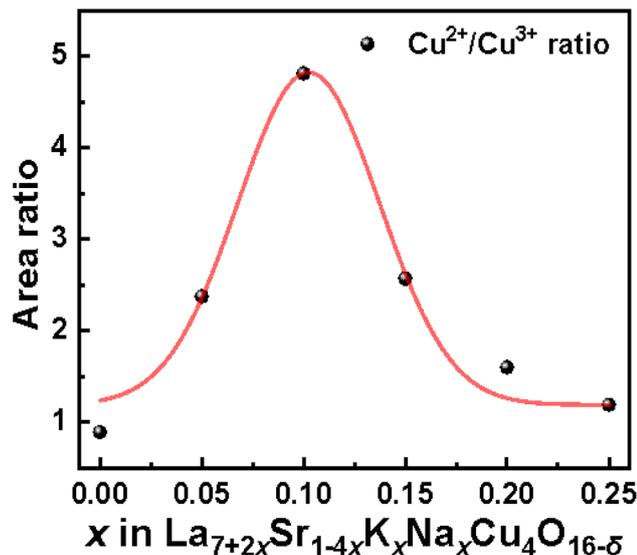
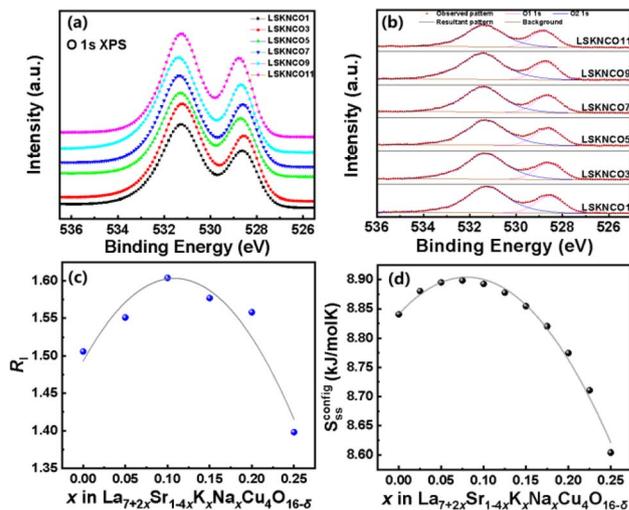**Fig. 6** Area ratio of Cu^{2+}/Cu^{3+} in $La_{7+2x}Sr_{1-4x}K_xNa_xCu_4O_{16-\delta}$.

Fig. 7 The O 1s XPS spectra (a), peak fitting of O 1s XPS spectra (b), ratio $I_{O2}^{1s} : I_{O1}^{1s}$ (c) of LSKNCO1, LSKNCO3, LSKNCO5, LSKNCO7, LSKNCO9 and LSKNCO11, and configurational entropy (d) of all the samples (LSKNCO1 to LSKNCO11).

substituted samples gradually increased in the doped samples to a maximum value of 4.882 at $x = 0.10$, followed by a gradual decrease, which indicates that the valence state of Cu firstly shifts from Cu^{3+} to Cu^{2+} and then moves back to Cu^{3+}. R. A. M. Ram *et al.* mentioned for the $(La, Ln)_{2-x}(Ba, Sr)_xCuO_{4-\delta}$ system that the substitution of La^{3+} with Sr^{2+} usually oxidizes Cu^{2+} to Cu^{3+}.[34] However, in the $La_{7+2x}Sr_{1-4x}K_xNa_xCu_4O_{16-\delta}$ system, the oxidation tendency caused by the replacement of two Sr^{2+} by one Na^+ and one K^+ is cancelled by the co-replacement of two Sr^{2+} by two La^{3+}. The change in the valence of Cu in the $La_{7+2x}Sr_{1-4x}K_xNa_xCu_4O_{16-\delta}$ system may be due to other reasons.

3.3 Oxygen vacancy in $La_{7+2x}Sr_{1-4x}K_xNa_xCu_4O_{16-\delta}$

The O 1s XPS spectra for all the investigated compositions are shown in Fig. 7a with two peaks at binding energies of 528.7 eV and 531.4 eV, denoted as O1 and O2, respectively. In the study on Ga^{3+}-doped $BiMn_{1-x}Ga_xO_3$-$BaTiO_3$ ceramics, K. K. Rahangdale[35] found that the two peaks at binding energies of 527.75 eV and 529.0–532.0 eV in the O 1s XPS spectra are related to the lattice oxygen without oxygen vacancies in the neighboring vicinity and vacancy-related oxygen with oxygen vacancies in the neighboring vicinity, respectively. Additionally, D. Kumar *et al.*[36] in Ti^{4+}-doped $La_{0.6}Ba_{0.4}Mn_{1-x}Ti_xO_3$ perovskites found the binding energies of lattice oxygen and vacancy related oxygen to be approximately 529.0–530.2 eV and 531.3–531.7 eV, respectively. Therefore, the binding energies O1 and O2 in our study may correspond to lattice oxygen without oxygen vacancies in the neighboring vicinity and vacancy related oxygen with oxygen vacancies in the neighboring vicinity, respectively.

Fig. 7b shows the fitted spectra of the two peaks of the selected samples. When $x \leq 0.10$, the intensity of the O2 peak (I_{O2}^{1s}) increases with increasing doping concentration of K and Na. However, there is a decreasing trend in the intensity of the O2 peak when $x > 0.10$. The $I_{O2}^{1s} : I_{O1}^{1s}$ ratio denoted by R_I for each sample is listed in Table 3 and shown in Fig. 7c. Compared to

Table 3 Binding energies (eV) of O1 and O2, the ratio $I_{O2}^{1s} : I_{O1}^{1s}$ (R_I) for $La_{7+2x}Sr_{1-4x}K_xNa_xCu_4O_{16-\delta}$

Sample	O1 1s	O2 1s	R_I
LSKNCO1	528.56	531.24	1.506
LSKNCO3	528.61	531.32	1.551
LSKNCO5	528.65	531.29	1.604
LSKNCO7	528.66	531.43	1.577
LSKNCO9	528.74	531.47	1.558
LSKNCO11	528.73	531.35	1.398

Fig. 6, the $I_{O2}^{1s} : I_{O1}^{1s}$ ratio can correspond well with the $Cu^{2+} : Cu^{3+}$ ratio, which means that the change in the valence of Cu in the $La_{7+2x}Sr_{1-4x}K_xNa_xCu_4O_{16-\delta}$ system is related to the change in the content of oxygen vacancies in the samples. In fact, as $La_{7+2x}Sr_{1-4x}K_xNa_xCu_4O_{16-\delta}$ is an equivalent doping system, it is natural that the $Cu^{2+} : Cu^{3+}$ ratio is directly related to the change in the oxygen vacancies. Therefore, the origin for the change in the $Cu^{2+} : Cu^{3+}$ ratio may be the same as the origin of the change in the $I_{O2}^{1s} : I_{O1}^{1s}$ ratio.

As shown in Fig. 3, the change in the lattice parameters of $La_{7+2x}Sr_{1-4x}K_xNa_xCu_4O_{16-\delta}$ is monotonous, which could not induce a parabolic change in the oxygen vacancies shown in Fig. 7c or a parabolic change in the $Cu^{2+} : Cu^{3+}$ ratio shown in Fig. 6 with the increase in the Na^+ and K^+ contents in the samples. Therefore, it is estimated that the change in the content of oxygen vacancies in $La_{7+2x}Sr_{1-4x}K_xNa_xCu_4O_{16-\delta}$ may be related to the configurational entropy change in this system with different amounts of Na and K doping. The configurational entropy can be calculated by the following equation.[37]

$$S_{ss}^{config} = -R\sum_i X_i \ln(X_i) \quad (2)$$

where R is the gas constant, and X_i is the mole fraction of each element. The calculated results for $La_{7+2x}Sr_{1-4x}K_xNa_xCu_4O_{16-\delta}$

are in the range of 1.03–1.07R (the details are listed in ESI†), which is consistent with the A_2BO_4-type medium entropy material (1–1.5R) discussed by M. Brahlek et al.[38] As shown in Fig. 7d, the entropy has a maximum at about $x \approx 0.10$ with Na and K doping variations, which is similar to the change in the $I_{O2}^{1s} : I_{O1}^{1s}$ ratio shown in Fig. 7c and the change in the $Cu^{2+} : Cu^{3+}$ ratio shown in Fig. 6. The change in the content of oxygen vacancies in $La_{7+2x}Sr_{1-4x}K_xNa_xCu_4O_{16-\delta}$ and the change in the $Cu^{2+} : Cu^{3+}$ ratio may be due to the change in the configurational entropy caused by the Na and K doping.

3.4 Superconducting properties of $La_{7+2x}Sr_{1-4x}K_xNa_xCu_4O_{16-\delta}$

Temperature-dependent resistivity measurements were conducted on all the samples from LSKNCO1 to LSKNCO11 in the temperature range from 2 to 120 K. The typical data for the samples LSKNCO1, LSKNCO5, LSKNCO8, and LSKNCO9 are shown in Fig. 8a–d (the others are presented in the ESI†).

For the samples LSKNCO1 to LSKNCO6, the resistivity decreases with decreasing temperature to show a metallic behavior until the temperature reaches T_c^{onset}. After T_c^{onset}, the resistivity drops sharply with a decrease in temperature. Subsequently, as the temperature continues to decrease, the resistivity reaches "zero" at T_c^{zero}. T_c^{onset} is not changed significantly for these six samples, which is about 38 K, as shown in Fig. 8e. However, as shown in Fig. 8f, the T_c^{zero} of $La_{7+2x}Sr_{1-4x}K_xNa_xCu_4O_{16-\delta}$ firstly increases and then decreases, which is a surprise at first glance. The main reason is that with an increase in the contents of Na and K in the sample, the average valence at the La site remains unchanged because the decrease tendency caused by the replacement of two Sr^{2+} with one Na^+ and one K^+ is cancelled by the replacement of two Sr^{2+}

with two La^{3+}. In this case, the valence of Cu should not change. Therefore, the T_c^{zero} of $La_{7+2x}Sr_{1-4x}K_xNa_xCu_4O_{16-\delta}$ should remain constant at about 16.5 K, as reported by L. Weckhuysen,[39] because most of us believe that the T_c^{zero} of doped $La_2CuO_{4-\delta}$ is strongly related to the valence of Cu, as indicated by P. G. Radaelli et al.[6] However, the XPS data shown in Table 2 in section 3.2 indicates that the $Cu^{2+} : Cu^{3+}$ ratio in $La_{7+2x}Sr_{1-4x}K_xNa_xCu_4O_{16-\delta}$ first increases and then decreases. This means that the amount of Cu^{3+} in $La_{7+2x}Sr_{1-4x}K_xNa_xCu_4O_{16-\delta}$ first decreases with an increase in x when $x < 0.100$, then increases when $0.100 < x < 0.25$. As mentioned by P. G. Radaelli et al.,[6] $La_{1.75}Sr_{0.25}CuO_{4-\delta/4}$ (which is corresponding to $La_{7+2x}Sr_{1-4x}K_xNa_xCu_4O_{16-\delta}$ with $x = 0.000$) is a hole over-doped superconductor. Therefore, the decrease in the holes (corresponding to the decrease in the Cu^{3+} content) in $La_{7+2x}Sr_{1-4x}K_xNa_xCu_4O_{16-\delta}$ with an increase in x when $x < 0.100$ will help to move to the optimal doped state. Then, the T_c^{zero} of $La_{7+2x}Sr_{1-4x}K_xNa_xCu_4O_{16-\delta}$ increases with an increase in x when $x < 0.100$. The T_c^{zero} of $La_{7+2x}Sr_{1-4x}K_xNa_xCu_4O_{16-\delta}$ decreases from 33.9 K for $x = 0.100$ to 26.7 K for $x = 0.125$, which can be due to the increase in the holes to move the sample back to the over-doped state.

With more Na and K doped into the sample, the metallic resistivity above T_c^{onset} for LSKNCO1 to LSKNCO6 changes to semiconductive resistivity for LSKNCO7 and LSKNCO8. This may be because the doping level directly affects the carrier concentration and metallic nature of the material. For samples LSKNCO1 ($x = 0$) and LSKNCO5 ($x = 0.1$), the doping level is low and the carrier concentration is sufficiently high to form effective conduction channels, which enhances the metallic properties. As the temperature decreases, superconductivity emerges, leading to increased carrier mobility and reduced

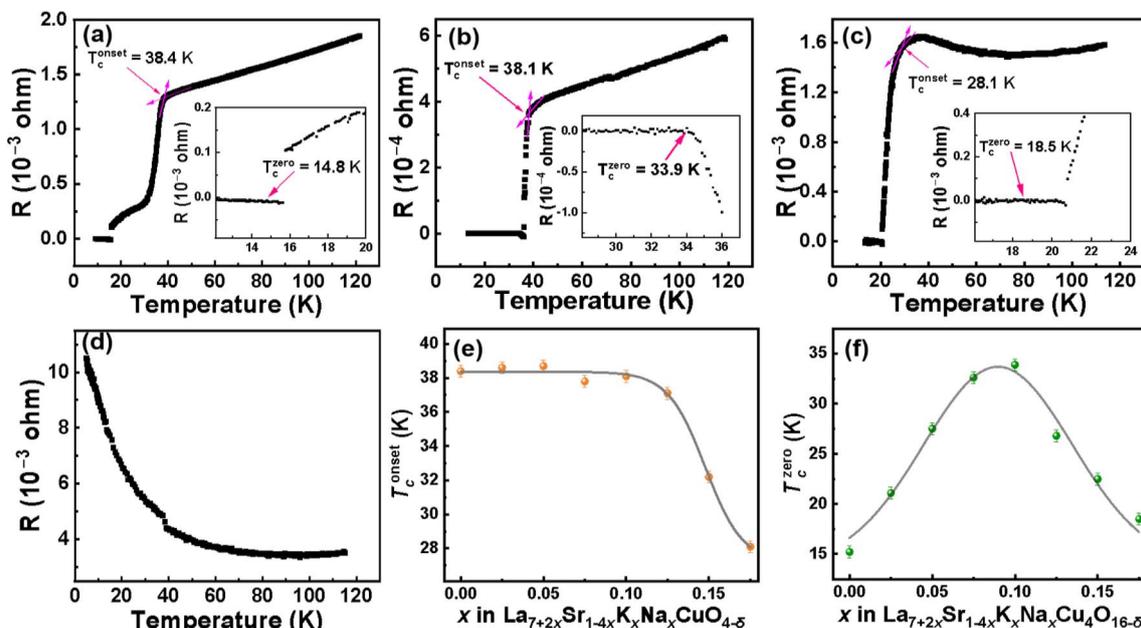
Fig. 8 Temperature-dependent resistance of LSKNCO1 (a), LSKNCO5 (b), LSKNCO8 (c), LSKNCO9 (d), T_c^{onset} ($0 \leq x \leq 0.175$) (e) and T_c^{zero} of the samples $La_{7+2x}Sr_{1-4x}K_xNa_xCu_4O_{16-\delta}$ ($0 \leq x \leq 0.175$) (f).

electron scattering, which results in a decrease in resistivity.[14,40] In contrast, for LSKNCO7 ($x = 0.15$) and LSKNCO8 ($x = 0.175$) (Fig. S18† and **8(c)**), the higher doping levels introduce increased disorder, leading to the presence of defects. This disorder enhances electron scattering, thereby hindering the decrease in resistivity, even though the materials exhibit superconductivity at low temperatures.[41] Additionally, the increased disorder due to higher doping levels may localize some carriers, preventing them from effectively contributing to conductivity at higher temperatures.[42] As the temperature decreases, these localized carriers contribute less to the metallic behavior, resulting in different resistivity characteristics compared to the lower-doped samples. T_c^{onset} decreases from 32.2 K for LSKNCO7 to 28.1 K for LSKNCO8, as shown in Fig. 8e, and T_c^{zero} continues to decrease from 22.5 K for LSKNCO7 to 18.5 K for LSKNCO8. The reason is similar to that for LSKNCO6, as mentioned above. It is noted that LSKNCO7 is tetragonal and LSKNCO8 is orthogonal, which means that the superconductivity can appear in both the tetragonal and orthogonal phases for the La$_{7+2x}$Sr$_{1-4x}$K$_x$Na$_x$Cu$_4$O$_{16-\delta}$ system.

With a further increase in the Na and K contents in the sample, "zero" resistivity is not be measured for the samples LSKNCO9 to LSKNCO11 with a semiconductive behavior for the temperature-dependent resistivity. The data for the temperature-dependent resistance of LSKNCO10 and LSKNCO11 is shown in Fig. S20–S21.†

In order to confirm the superconductivity of the La$_{7+2x}$Sr$_{1-4x}$K$_x$Na$_x$Cu$_4$O$_{16-\delta}$ system, the magnetization of the samples was measured under a magnetic field of 10 Oe in the temperature range of 2–300 K. Typical data are shown in Fig. 9 and the data for other samples are presented in ESI (Fig. S13–S21†). As the temperature decreases, the magnetization of the samples starts to decrease to negative values at T_c^{mag}, which are 37.5 K and 28.0 K for LSKNCO5 and LSKNCO8, respectively. They both exhibit strong diamagnetic signals, confirming that superconductivity exists in these samples as "zero" resistivity is already observed above. Weak diamagnetic signals (about 2% to 0.1% of that for LSKNCO5 or LSKNCO8) are found in the magnetization of the samples for LSKNCO9 to LSKNCO11. Since the sample LSKNCO9 no longer exhibits "zero" resistivity, the temperature-dependent DC magnetization data (Fig. S19†) reveals that the zero-field-cooling (ZFC) and field-cooling (FC)

curves do not show any splitting, which may be attributed to weak flux pinning in the material.[43] This observation further suggests the absence of superconductivity properties in the sample. Additionally, the incomplete diamagnetic signals observed in the magnetic susceptibility measurements of LSKNCO10 and LSKNCO11 further corroborate the loss of superconductivity in these materials.

As discussed in section 3.3, the change in the Cu^{2+} : Cu^{3+} ratio is due to the change in the configurational entropy caused by the Na and K doping in the present equivalent doping La$_{7+2x}$Sr$_{1-4x}$K$_x$Na$_x$Cu$_4$O$_{16-\delta}$ system. Therefore, the T_c^{zero} of La$_{7+2x}$Sr$_{1-4x}$K$_x$Na$_x$Cu$_4$O$_{16-\delta}$ is increased to 33.9 K (for $x = 0.10$) from 14.8 K (for $x = 0.00$) and then lowered to 18.5 K (for $x = 0.175$), which is related to the change in the configurational entropy caused by Na and K doping.

4. Conclusions

In summary, we demonstrated the synthesis of new series of solid solutions La$_{7+2x}$Sr$_{1-4x}$K$_x$Na$_x$Cu$_4$O$_{16-\delta}$ ($0.00 \leq x \leq 0.25$) by the traditional solid-state method, which crystalizes in the $I4/mmm$ space group when $0.00 \leq x < 0.16$ and $Fmmm$ when $0.16 < x \leq 0.25$.

All the tetragonal phase La$_{7+2x}$Sr$_{1-4x}$K$_x$Na$_x$Cu$_4$O$_{16-\delta}$ ($0.00 \leq x < 0.16$) are superconductors with T_c^{zero} increasing from 14.8 K for $x = 0.00$ to 33.9 K for $x = 0.10$ and then decreasing to 22.5 K for $x = 0.15$. The change in the T_c^{zero} for the equivalent doping system La$_{7+2x}$Sr$_{1-4x}$K$_x$Na$_x$Cu$_4$O$_{16-\delta}$ is related to the change in the Cu^{2+} : Cu^{3+} ratio in the samples confirmed by the XPS data, which may be caused by the change in the configurational entropy.

T_c^{zero} for the orthogonal phase La$_{7+2x}$Sr$_{1-4x}$K$_x$Na$_x$Cu$_4$O$_{16-\delta}$ with $x = 0.175$ is about 18.5 K. The other samples with $x = 0.200$, 0.225, and 0.250 do not show superconductivity in the present study.

Data availability

The data supporting this article have been included as part of the ESI.† All relevant data are available from the corresponding author upon reasonable request.

Author contributions

Deyang Xu: methodology, data curation, writing—original draft preparation; Guohong Cai: conceptualization; Peiliang Huang: formal analysis; Xi Wu: formal analysis; Yan Wang: data curation; Jinling Geng: conceptualization; Jing Ju: methodology, data curation; Xiaoge Wang: investigation, formal analysis; Congling Yin: conceptualization, supervision, project administration, writing—review and editing; Guobao Li: conceptualization, formal analysis, supervision, writing—review and editing. All authors have read and agreed to the published version of the manuscript.

Conflicts of interest

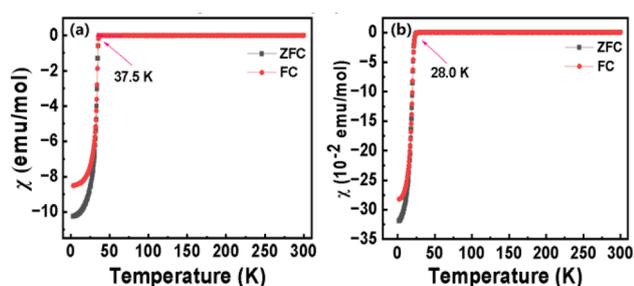There are no conflicts to declare.

Fig. 9 Temperature dependence of DC magnetic susceptibility of LSKNCO5 (a) and LSKNCO8 (b) in an applied field of 10 Oe after zero field cooling.

Acknowledgements

References

1 J. G. Bednorz and K. A. Mller, *Z. Phys. B*, 1986, **64**, 189–193.
2 Y. Maeno, A. Odagawa, N. Kakehi, T. Suzuki and T. Fujita, *Physica C*, 1991, **173**, 322–330.
3 M. Onoda, S. Shamoto, M. Sato and S. Hosoya, *Jpn. J. Appl. Phys.*, 1987, **26**, L363–L365.
4 J. C. Grenier, A. Wattiaux, N. Lagueyte, J. C. Park, E. Marquestaut, J. Etourneau and M. Pouchard, *Physica C*, 1991, **173**, 139–144.
5 B. Dabrowski, Z. Wang, J. D. Jorgensen, R. L. Hitterman, J. L. Wagner, B. A. Hunter and D. G. Hinks, *Physica C*, 1993, **217**, 455–460.
6 P. G. Radaelli, D. G. Hinks, A. W. Mitchell, B. A. Hunter, J. L. Wagner, B. Dabrowski, K. G. Vandervoort, H. K. Viswanathan and J. D. Jorgensen, *Phys. Rev. B*, 1994, **49**, 4163–4175.
7 J. B. Torrance, Y. Tokura, A. I. Nazzal, A. Bezinge, T. C. Huang and S. S. P. Parkin, *Phys. Rev. Lett.*, 1988, **61**, 1127–1130.
8 J. P. Attfield, A. L. Kharlanov and J. A. McAllister, *Nature*, 1998, **394**, 157–159.
9 J. B. Torrance, A. Bezinge, A. I. Nazzal, T. C. Huang, S. S. P. Parkin, D. T. Keane, S. J. LaPlaca, P. M. Horn and G. A. Held, *Phys. Rev. B*, 1989, **40**, 8872–8877.
10 J. M. Tarascon, L. H. Greene, W. R. McKinnon and G. W. Hull, *Solid State Commun.*, 1987, **63**, 499–505.
11 K. Oh-Ishi and Y. Syono, *J. Solid State Chem.*, 1991, **95**, 136–144.
12 B. Büchner, M. Braden, M. Cramm, W. Schlabitz, O. Hoffels, W. Braunisch, R. Müller, G. Heger and D. Wohlleben, *Physica C*, 1991, **185–189**, 903–904.
13 M. A. Subramanian, J. Gopalakrishnan, C. C. Torardi, T. R. Askew, R. B. Flippen, A. W. Sleight, J. J. Lin and S. J. Poon, *Science*, 1988, **240**, 495–497.
14 Y. Liu, Y. Wang, Y. Cai, Z. Hao, X.-M. Ma, L. Wang, C. Liu, J. Chen, L. Zhou, J. Wang, S. Wang, H. He, Y. Liu, S. Cui, B. Huang, J. Wang, C. Chen and J.-W. Mei, *Phys. Rev. Mater.*, 2023, **7**, 064801.
15 Y. Zhao, W. Deng, X. Chen, H. Zhang, A. Chang and Y. Xie, *J. Mater. Sci.: Mater. Electron.*, 2022, **33**, 22448–22455.
16 D. Lv, R. Zuo and S. Su, *J. Mater. Sci.: Mater. Electron.*, 2011, **23**, 1367–1372.
17 J. B. Goodenough, J. S. Zhou and K. Allan, *J. Mater. Chem.*, 1991, **1**, 715–724.
18 A. F. Dong, H. X. Geng, G. C. Che, W. W. Huang, S. L. Jia and Z. X. Zhao, *Supercond. Sci. Technol.*, 2006, **19**, 206–211.
19 R. Li, X. Wu, Z. Chen, Y. Qian, C. Zhu, H. Wei, S. Wang, J. Sha and J. Xia, *Phys. Lett. A*, 1990, **144**, 35–38.
20 A. Malinowski, M. Z. Cieplak, M. Berkowski, W. Plesiewicz and T. Skośkiewicz, *Acta Phys. Pol., A*, 2006, **109**, 617–621.
21 C. Zhang and Y. Zhang, *J. Phys.: Condens.Matter*, 2002, **14**, 9659–9665.
22 C. J. Zhang and H. Oyanagi, *Physica C*, 2008, **468**, 1155–1158.
23 A. Coelho, *Coelho Software*, 2012.
24 C. Wang and T. Hughbanks, *Inorg. Chem.*, 2002, **34**, 5524–5529.
25 A. Kimura, M. Kawate, H. Hasegawa and T. Suzuki, *Surf. Coat. Technol.*, 2003, **169–170**, 367–370.
26 J. M. Tarascon, L. H. Greene, W. R. McKinnon, G. W. Hull and T. H. Geballe, *Science*, 1987, **235**, 1373–1376.
27 H. Wang, C.-H. Wang, G. Li, T. Jin, F. Liao and J. Lin, *Inorg. Chem.*, 2010, **49**, 5262–5270.
28 H. Wang, C. Yang, J. Lu, M. Wu, J. Su, K. Li, J. Zhang, G. Li, T. Jin, T. Kamiyama, F. Liao, J. Lin and Y. Wu, *Inorg. Chem.*, 2013, **52**, 2388–2392.
29 Y. Foucaud, M. Badawi, L. O. Filippov, O. Barres, I. V. Filippova and S. Lebegue, *Chem. Sci.*, 2019, **10**, 9928–9940.
30 Y. Lu, Y. Cai, Q. Zhang, L. Liu, Z. Niu and J. Chen, *Chem. Sci.*, 2019, **10**, 4306–4312.
31 S. Yadav, D. Kumar and A. K. Singh, *Mater. Today Commun.*, 2024, **38**, 107767.
32 C. S. Gopinath, *J. Chem. Soc., Faraday Trans.*, 1996, **92**, 3605–3610.
33 U. M. Meshiya, P. Y. Raval, P. R. Pansara, M. Nehra, N. Jakhar, S. Kumar, K. B. Modi, D.-K. Lim and R. K. Singhal, *Ceram. Int.*, 2020, **46**, 2147–2154.
34 R. A. M. Ram, P. Ganguly and C. N. R. Rao, *Phase Transitions*, 2006, **10**, 107–121.
35 K. K. Rahangdale and S. Ganguly, *Phys. B*, 2022, **626**, 413570.
36 D. Kumar and A. K. Singh, *J. Phys. Chem. Solids*, 2023, **176**, 111253.
37 O. F. Dippo and K. S. Vecchio, *Scr. Mater.*, 2021, **201**, 113974.
38 M. Brahlek, M. Gazda, V. Keppens, A. R. Mazza, S. J. McCormack, A. Mielewczyk-Gryń, B. Musico, K. Page, C. M. Rost, S. B. Sinnott, C. Toher, T. Z. Ward and A. Yamamoto, *APL Mater.*, 2022, **10**, 110902.
39 L. Weckhuysen, J. Vanacken, P. Wagner and V. V. Moshchalkov, *Eur. Phys. J. B*, 2002, **29**, 369–375.
40 C. Collignon, B. Fauqué, A. Cavanna, U. Gennser, D. Mailly and K. Behnia, *Phys. Rev. B*, 2017, **96**, 224506.
41 M. Qin, R. Zhang, C. Miao, Z. Wei, Y. Shi, Y. Yao, H. Wang, Y. Li, K. Jin and X. Xiang, *Phys. Rev. Res.*, 2024, **6**, 023194.
42 Z.-X. Li, S. A. Kivelson and D.-H. Lee, *npj Quantum Mater.*, 2021, **6**, 36.
43 H. Chauhan and G. D. Varma, *J. Appl. Phys.*, 2024, **135**, 013901.